

## An investigation of Structural Properties of Monometallic (Ag, Pd) and Bimetallic (Ag@Pd) Nanoparticles Growth on Macro Porous Silicon

Duaa A. Hashim<sup>1</sup>, Alwan M. Alwan<sup>1\*</sup> and Muslim F. Jawad<sup>1</sup>

<sup>1</sup>Department of Applied Sciences, University of Technology, Baghdad, Iraq.

Received 23 April 2018; Revised 8 May 2018; Accepted 17 May 2018

### ABSTRACT

Monometallic nanoparticle Ag, Pd and bimetallic nanoparticles Ag@Pd with well-controlled morphology, uniform size, and regular alloy structure were produced by an ion reduction process with dangling bonds of porous layer Psi to fabricate monometallic(Ag, Pd) /macro Psi and bimetallic (Ag@Pd) /macro Psi hetro-structure. Psi substrate was synthesized by Photo-electrochemical etching (PECE) with a laser power density (15 mW/cm<sup>2</sup>), monometallic structure has been synthesized by dipping fresh Psi sample in salt solutions (AgNO<sub>3</sub> and PdCl<sub>2</sub>) for about 5 min, while bimetallic nanoparticles was synthesized by dipping Psi in mix solution at a ratio (1:1) for about 2 and 4 min. The monometallic and bimetallic nanoparticles were confirmed by scanning electron microscopy (SEM), X-ray diffraction (XRD) and energy dispersive X-ray analysis (EDS). The results show that the composition of Ag@Pd alloy nanoparticles was uniformly dispersed and well-defined distribution on Psi surface; having an average size of (8 to 7.1) nm is smaller than monometallic nanoparticles sizes. The lower Ag@PdNPs size and therefore a higher specific surface area (S.S.A) were obtained for about (71 to 63.8) m<sup>2</sup>/g<sub>m</sub>, these high specific area is most important for different application such as: chemicals or gas sensing.

**Keywords:** Ag@Pd; Ion Reduction Process; Monometallic; Bimetallic; PECE; Sensing Performances; S.S.A.

### 1. INTRODUCTION

Psi was fabricated by photo-electrochemical etching (PECE) process as results from the interaction Si-H dangling bonds groups on the surface of the Psi are fragmented and the amount of the silicon dangling bonds increase [1]. Psi layer which can be easily modified by dissimilar noble-metal nanoparticles, noble-metal nanoparticles deposited on porous silicon Psi by the immersion plating method [2,3] but also the thermal decomposition method [4]. Bimetallic nanoparticles (NPs) that consist of two different noble metal elements; have long been receiving considerable attention due to their distinct physicochemical properties related to monometallic nanoparticles [5]. Bimetallic nanoparticles frequently show greater catalytic performances than the monometallic nanoparticles due to interactive effect between two different metals and greater tunability in chemical compositions and structures [6]. Recently, the preparation of metallic nanoparticles with various compositions, structures, shapes and sizes [7–8]. Due to their unusual chemical and physical properties, they are expected to have potential applications in many technologies, such as opt-electronic Nano devices, catalysts, and chemical sensors [9].

---

\*Corresponding Author: alkrzsm@yahoo.com

In this paper, hybrid structure was fabricated by two step process, the first step Photo-electrochemical etching (PECE) to prepare Psi as a substrate, the second step (ion reduction process) to prepare hetro-structure by depositing monometallic and bimetallic on Psi.

## 2. EXPERIMENTAL PART

### 2.1 Preparation of Psi Substrate

Psi was prepared by Photo electrochemical etching (PECE) method from silicon wafer n-type (100) oriented with resistivity (10Ω/cm). The substrate was etched in the electrolyte consisted of Hydrofluoric acid (1 HF 48%) to 1 Ethanol (C<sub>2</sub>H<sub>5</sub>OH 99.9%), HF concentration in the solution is 24%, with etching current density of about 20mA/cm<sup>2</sup>. The illumination conditions involving laser power density 15 mW/cm<sup>2</sup> of 635 nm wavelength for 15 min etching time. After the etching process, substrates were kept in methanol to prevent oxidizing, the experimental setup is shown in figure (1).

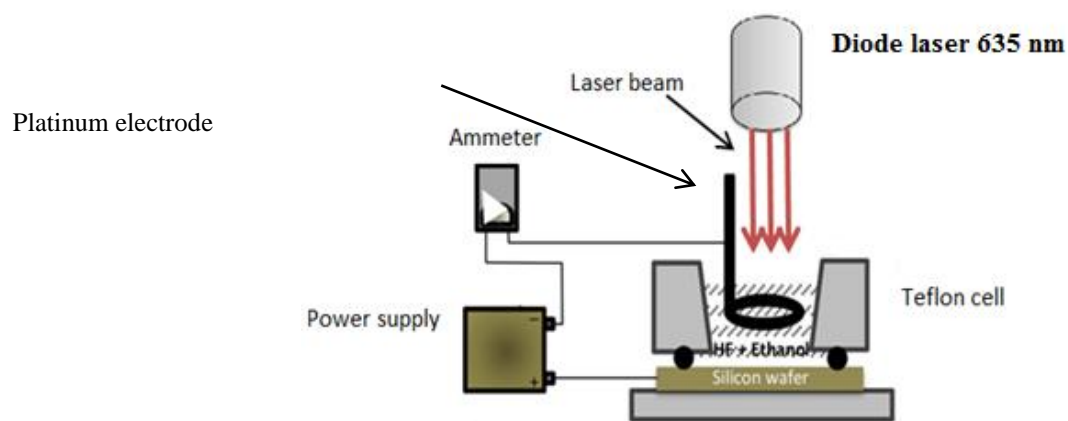


**Figure 1.** Setup of photo electrochemical etching (PECE) process.

### 2.2. Synthesis Monometallic (Ag,Pd) /Macro Psi and Bimetallic Ag@Pd/Macro Psi Hetro Structure

Chemical salt solutions of Ag and Pd were fabricated using 1 mM AgNO<sub>3</sub> diluted in distilled water and 0.15 M HF, 1 mM PdCl<sub>2</sub>, and a few drops of HCl with concentration 37% at 60° C under magnetic stirring for about 30min. Hetro-structure monometallic was fabricated by dipping Psi in the solution of AgNO<sub>3</sub> and PdCl<sub>2</sub> for 5 min, while bimetallic alloy Ag@PdNPs/macro Psi hetro-structure was fabricated by mixing of two solutions at a ratio of (1:1) with immersion time of about 2 and 4 min. The required solution concentrations were prepared using the following equation [10]:

$$\text{Molarity} = \frac{W}{\frac{M.Wt}{V}} \quad (1)$$

Where W (gm.) is the weight of the AgNO<sub>3</sub> and PdCl<sub>2</sub>, M.Wt of AgNO<sub>3</sub> and PdCl<sub>2</sub> is about 169.8731 and 177.33 (gm. /mole), respectively, and V is the volume of the dissolved solution. The ion reduction deposition of Ag and Pd occurs according to the following reactions, respectively [11, 12]:



Psi substrate was immersed in mix salt solution for 2 and 4 min at room temperature. The procedures for growth bimetallic alloys Ag@Pd NPs/macroPsi hetero structures are shown in figure (2).

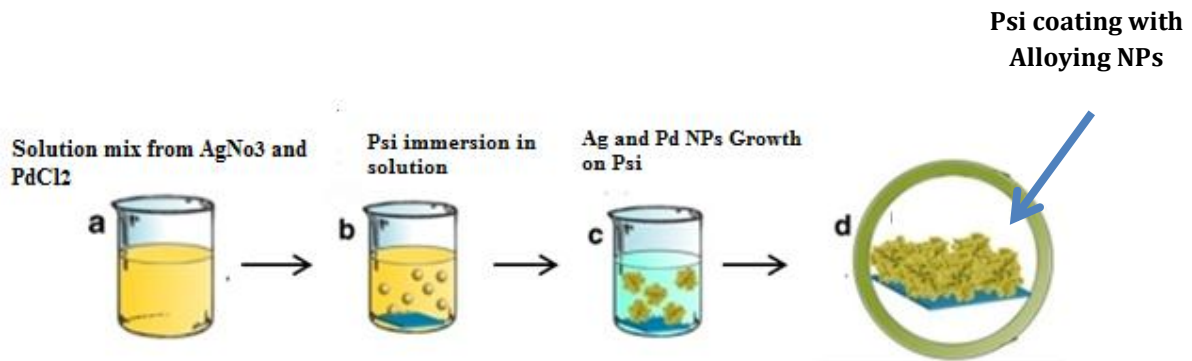


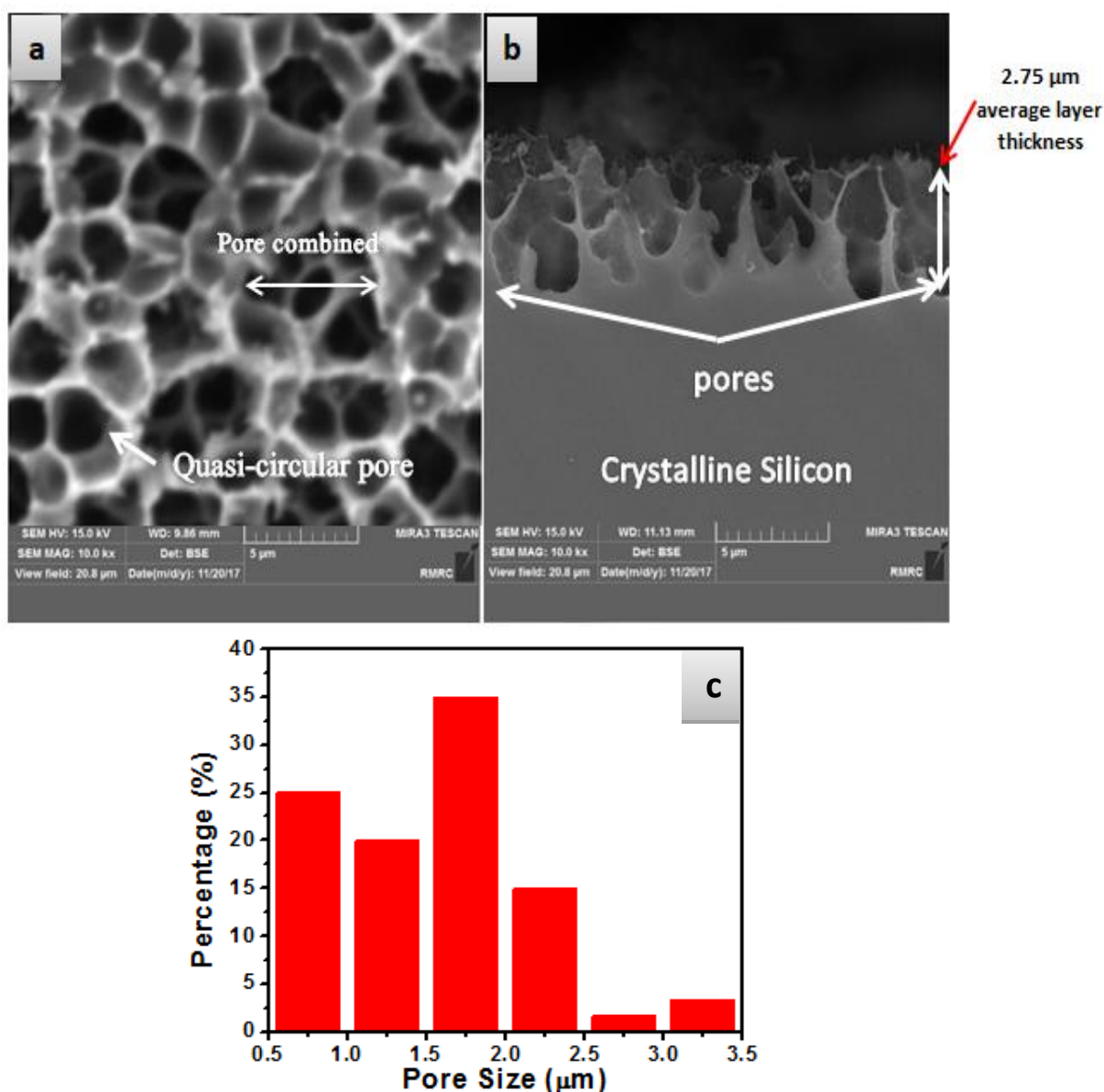
**Figure 2.** Procedure for synthesis bimetallic alloy Ag@Pd NPs (a) synthesis solution with two metal (Ag and Pd); (b) bare Psi dips in mix solution; (c) growth NPs on the surface of Psi (d) finally, Ag@Pd alloy NPs deposited on Psi.

The morphological properties of the monometallic and bimetallic NPs were studied by SEM (MIRA3 TESCAN) in the Razi metallurgical research center – Iran, XRD and EDS analyses.

### 3. RESULTS AND DISCUSSION

#### 3.1 Characterization of Bare Psi Substrate

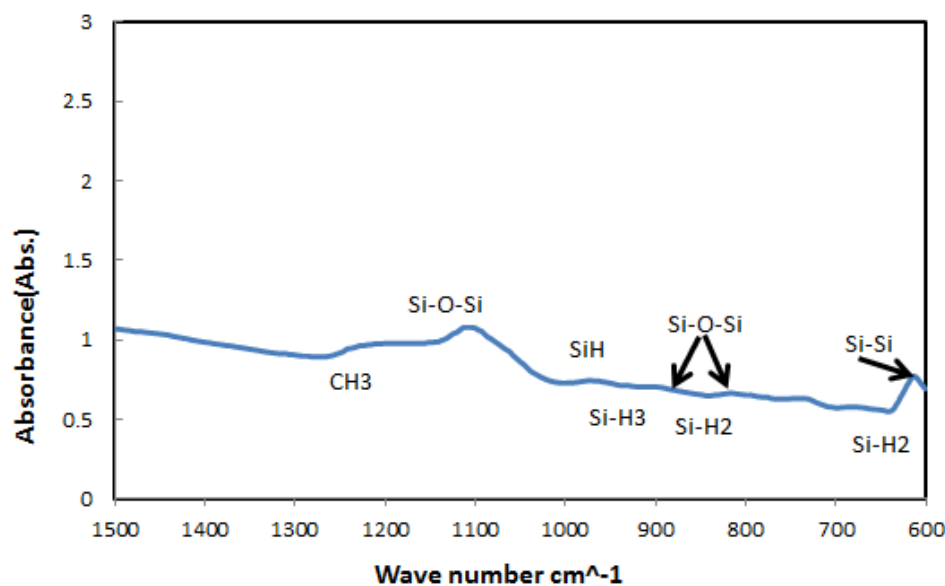
The surface morphology of bare Psi layer before combining monometallic and bimetallic nanoparticles (Ag@Pd) is shown in figure (3, a) shows Psi substrate appears as a pore-like structure, and the pores have a cylinder-shaped which randomly distributed, perpendicularly oriented to the sample phase. A rise in pore size has also pored overlapping lead to change pore shapes from rounded to random shaped pores, pore overlapping was appeared with high laser intensity to increase the dissolution of thin pore walls which lead to pore combined [13] Figure (3, b) shows a cross-section of bare Psi, in which the pores cross section is non-uniform along the depth and the average layer depth is about 2.75  $\mu\text{m}$ . Figure (3, c) shows the statistical distribution of pore size is about 0.75 to 3.25  $\mu\text{m}$  and the peak of the distribution occurs at 1.75  $\mu\text{m}$ , porosity of bare Psi around (48%).



**Figure 3.** (a) SEM images of bare macroPsi surface morphology (b) Cross – sectional SEM image and (c) The statistical distribution of pore sizes of Psi.

### 3.2 Fourier Transform Infrared (FTIR) Of Bare Macro Psi Substrate

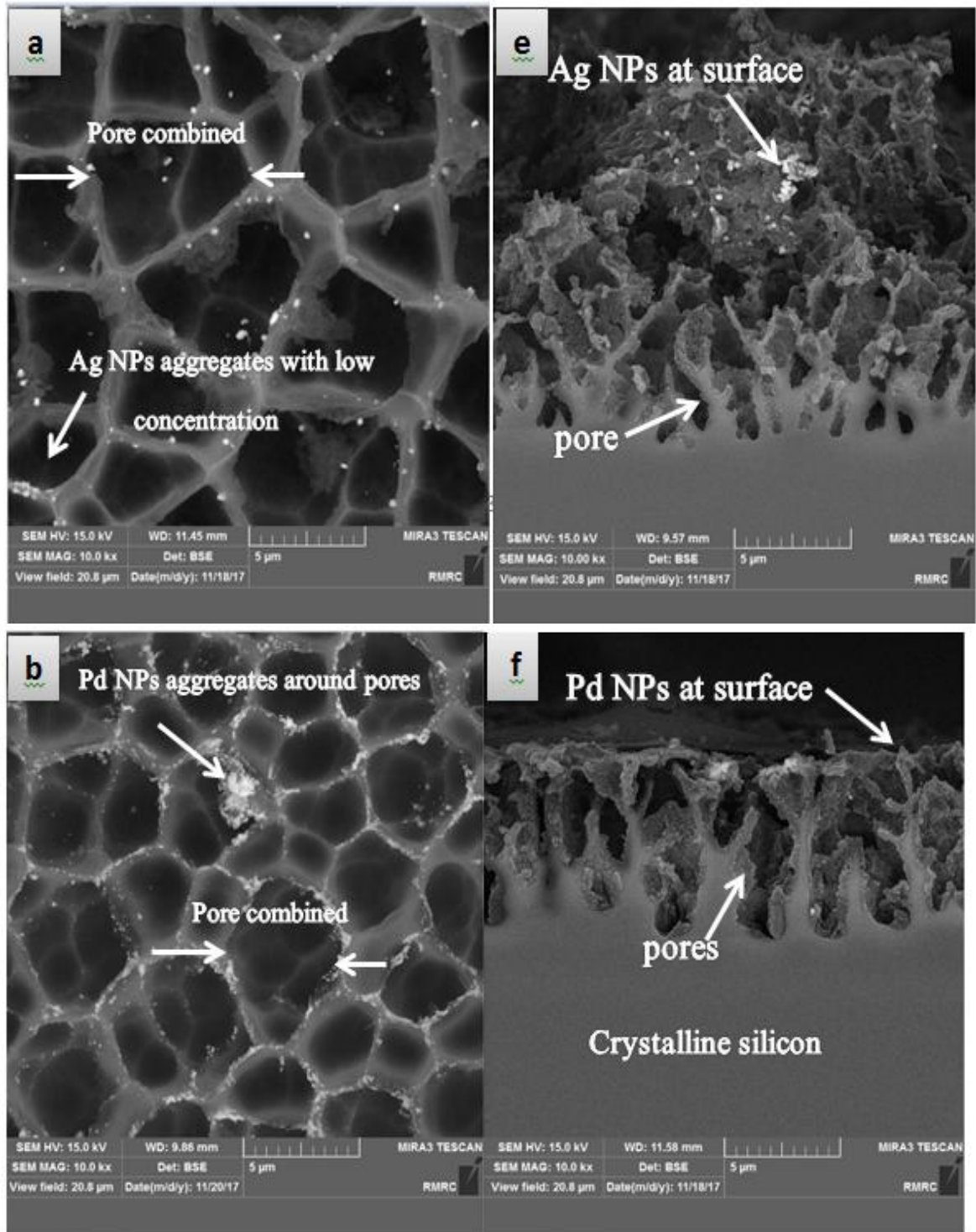
Chemical composition of the Psi matrix was studied by using FTIR spectroscopy technique which describes the predominance of elements such as hydrogen, oxygen and Si-H groups (growth sites). The peaks existing in the spectra, respectively corresponded to: Si-O-Si located at  $1106\text{ cm}^{-1}$ ,  $975\text{ cm}^{-1}$  for monohydrides Si-H in Bending mode,  $(600-800)\text{ cm}^{-1}$  attributed to the dihydrides Si-H<sub>2</sub> (wagging bonds),  $945\text{ cm}^{-1}$  at trihydrides Si-H<sub>3</sub> and asymmetric deformation CH<sub>3</sub> at  $1210$ . Psi substrate is simply oxidized under ambient environments to form a non-conductive oxide layer on the surface. As shown in fig. below (4).



**Figure 4.** FTIR absorbance spectra of bare macro Psi

### 3.3 Characterization of Ag, Pd NPs/Macro Psi and Ag@Pd NPs/Macro Psi

Reducing process of Ag and Pd ions with dangling bonds of porous matrix is an active method to form hetero structure monometallic Ag NPs/macro psi, Pd NPs/ macro Psi and bimetallic alloy Ag@Pd NPs/macro Psi [14,11]. The density, the size and the arrangement of the Ag NPs, Pd NPs and Ag@Pd NPs depend on the morphology of the essential Psi [15]. Figure 5 (a-d), illustrates the SEM images of monometallic Ag,Pd NPs/macro Psi and Ag@Pd NPs/macro Psi hetero structure. In figure 5 (a, b), represent the growth Ag and Pd NPs on Psi, Nanoparticles-aggregates around pores in the macro-Psi surface. The Ag NPs was deposited with the distribution in size ranging from 25 to 325 nm, and the peak is about 125 nm with percentage 15.135 %, while Pd NPs was deposited with the distribution in size ranging from 50 to 290 nm, and the peak is about 70 nm with percentage 39%. Figure5 (c and d), shows the SEM images of bimetallic Ag@Pd NPs/macro Psi hetero structure with ratio 1:1. It is clear that the formed Ag@Pd nanoparticles are highly uniform spread outside the walls of silicon inside the porous matrix, nanoparticles are arranged like (ice) between trenches. The distribution was various from 30 to 250 nm and the peak is about 30 nm, while in figure 5 (d) for the sample was dipping at 4 min, it can be defined, distinguished that the particles are greatly aggregation around and inside pores over the porous silicon surface, so the pores are fully covered by Ag@PdNPs, and formed two layers (lower and upper) around the pore. The distribution varied from 75 to 425 nm and the peak is about 75 nm. Fig. 5 (e-h) cross-sectional SEM images, from these figures, it is easy to distinguish that the nanoparticles are positioned outside or inside the pores like cotton. Ag@PdNPs/macro Psi decorates the inside of the pore walls. The as-prepared Ag, Pd NPs and Ag@PdNPs were described by Scanning electron microscopy. Fig. (6) Statistical distribution of pore sizes of Psi. The deposited nanoparticles can be classified into two forms: silver and palladium nanoparticles with small average sizes dispersed on the tops and sides of the pores in the porous structures, and those with large Nano sizes (aggregation); aligned along the pore (inside each pore) [16].



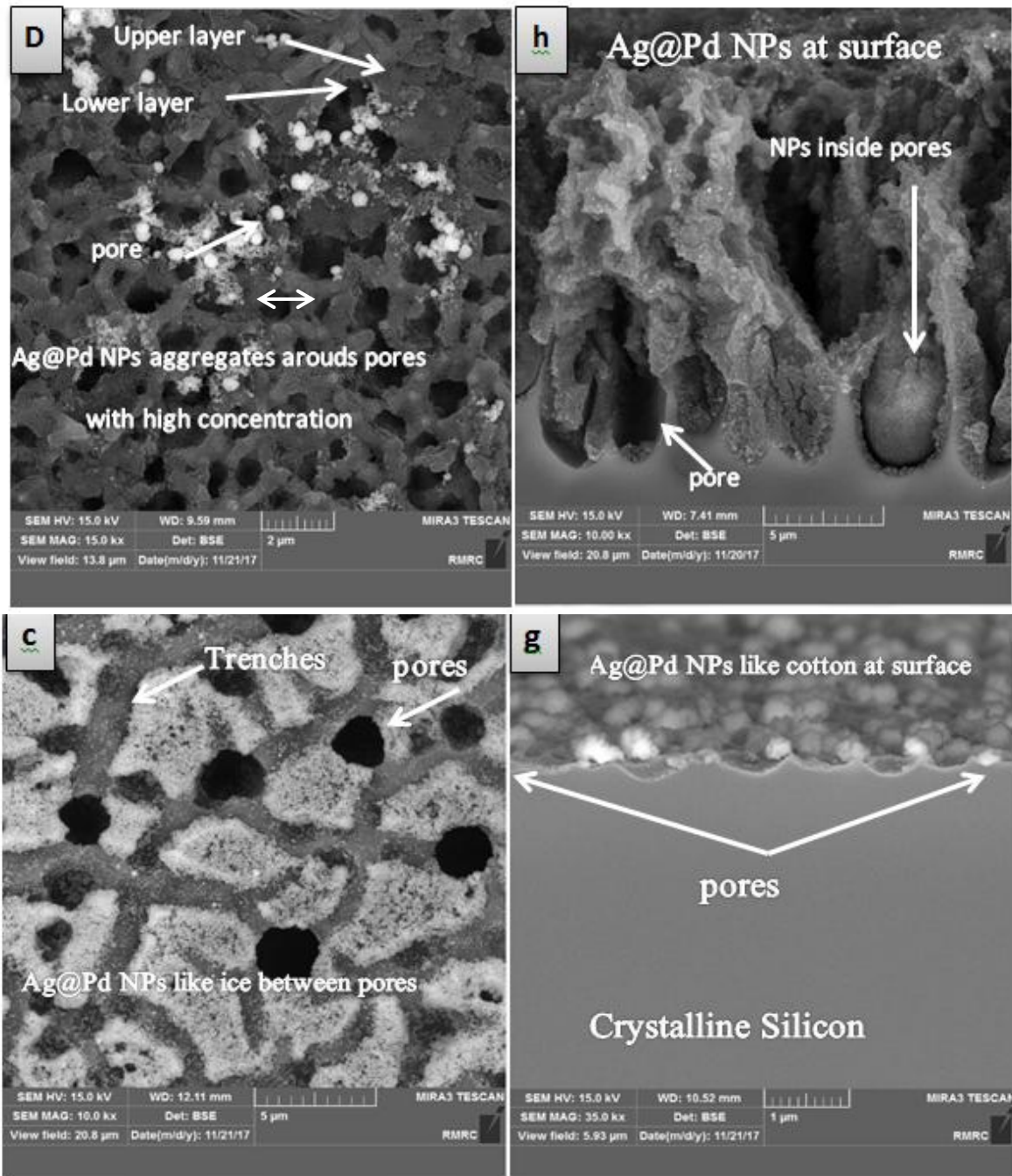


**Figure 5.** (a-d) SEM images of (a) Ag/macro Psi, (b) Pd/macro Psi ,(c) Ag@Pd/macro Psi at 2 min and (d) Ag@Pd/macro Psi at 4 min, (e-h) cross – sectional SEM image.

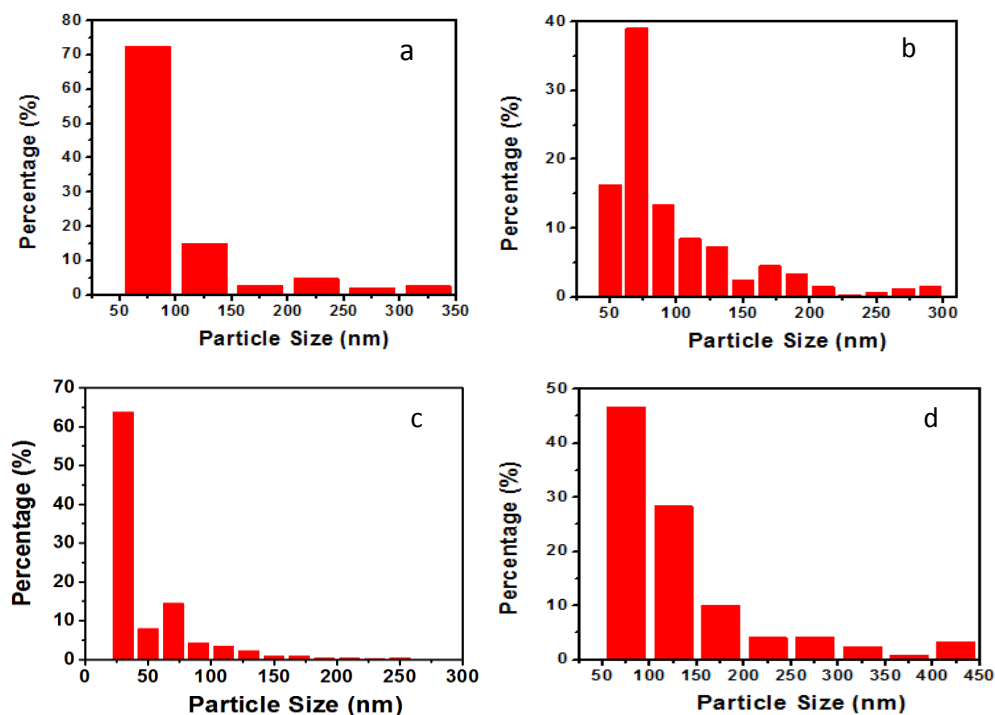


**Figure 6.** (a-d) statistical distribution of the (a) Ag NPs sizes, (b) Pd NPs sizes, (c) Ag@PdNPs at 2 min and (d) Ag@PdNPs at 4 min.

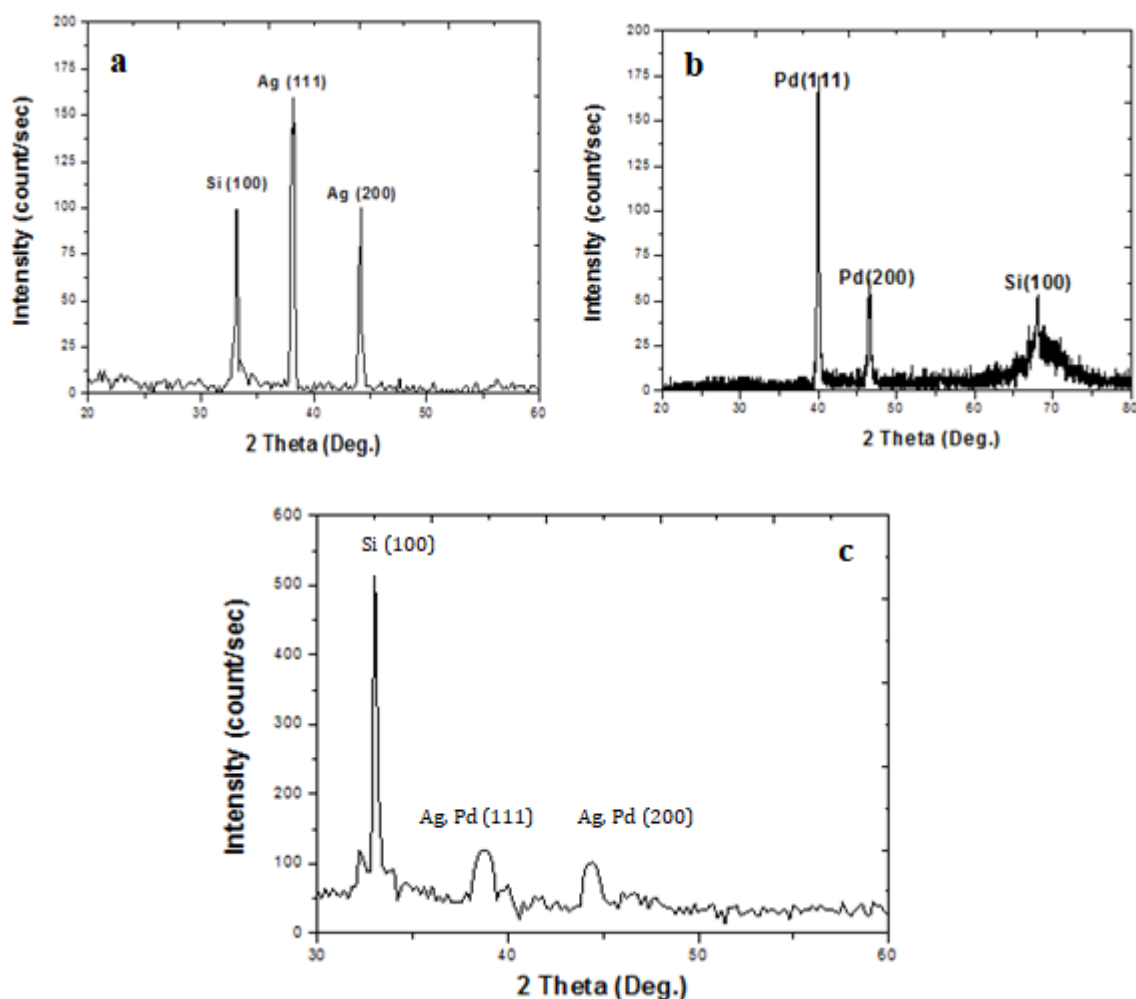
XRD is an effective device to discover the structure of NPs, especially for bimetallic NPs [17]. The XRD spectra of all NPs samples are assembled in Figure 7. For monometallic Ag NPs, the intense peaks at  $38.18^\circ$  and  $44.18^\circ$ . This result is in a good agreement with the results reported in the works [18] and Pd NPs planes at  $39.9^\circ$  and  $46.53^\circ$  these peaks which are conformity with reference data (JCPDS numbers 271402) [19]. The plane reflections (111) and (222) of Ag and Pd cubic (FCC) crystal. XRD patterns of the Ag@Pd bimetallic NPs, the diffraction peaks are located at  $39^\circ$  and  $45^\circ$  show that the observed diffraction peaks are among those of Ag and Pd, suggesting the formation of alloy NPs [20]. The crystalline size of NPs was calculated Sherres equation [21]. Bimetallic Ag@Pd alloy NPs have XRD peaks is wider than that of monometallic Ag and Pd nanoparticles. This result is due to similarity of lattice constant of silver and palladium nanoparticles for about  $4.079$  and  $3.859 \text{ \AA}$ , respectively, so that Ag@Pd bimetallic NPs has overlap of XRD peaks [4]. The specific surface area (S.S.A) of nanoparticles it is known as [15]:

$$S.S.A. = \frac{6000}{D * \rho} \quad (4)$$

Density of monometallic Ag and Pd ( $10.5$  and  $12.023$ )  $\text{g/cm}^3$ , correspondingly, whereas the density of bimetallic alloys Ag@Pd NPs  $11.548\text{g/cm}^3$ , value of density for Ag@Pd NPs can be determined using equation depending on EDS analysis results [13]:

$$D = \frac{a * \rho + b * \rho}{a + b} \quad (5)$$

Where  $\rho$  is the density of the monometallic Ag and Pd NPs,  $D$ = density of Ag@Pd bimetallic alloy nanoparticles  $\text{g/cm}^3$ ,  $a$  = wt. % Ag and  $b$  = wt. %Pd.



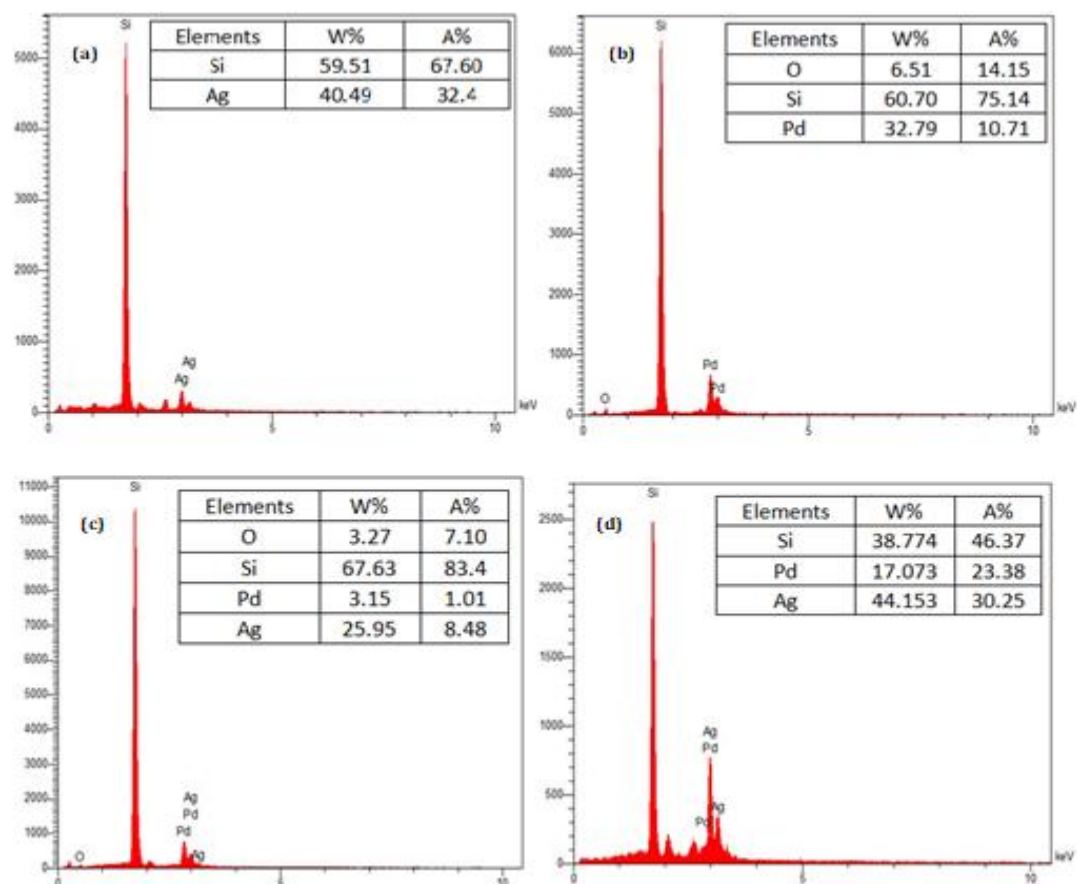
**Figure 7.** XRD Spectra of (a) Ag NPs/Macro Psi (b) Pd NPs/Macro Psi and (c) Ag@Pd NPs/Macro Psi

Table 1, demonstrates the grain size of the monometallic and bimetallic NPs in the phase (111) and (200) on Psi sample. The Ag@Pd bimetallic NPs have lower size and hence higher S.S.A was obtained related to monometallic Ag, Pd NPs.

**Table 1** Particle size and specific surface area (S.S.A) of monometallic Ag, Pd NPs and bimetallic alloy Ag@Pd NPs

Nanoparticles	Phase (111)		Phase (200)	
	Nanoparticles Size (nm)	S.S.A. (m <sup>2</sup> /g <sub>m</sub> )	Nanoparticles Size (nm)	S.S.A (m <sup>2</sup> /g <sub>m</sub> )
Ag NPs	21.61	26.4	31.3	18.3
Pd NPs	26.32	16.85	29.62	18.96
Ag@Pd alloy NPs	7.3	71	8	63.8

EDS was used to give the indication of the surface structure Psi due to the depositing by metallic nanoparticles. Figure 8 (a, b, c and d) displays the existence of Ag, Pd and Ag@Pd with ratio 1:1 on the Psi sample, the intensity of monometallic PdNPs peak is lower than that of monometallic Ag NPs and bimetallic alloy Ag@PdNPs at 4 min indicating higher deposition rate from Ag@PdNPs bimetallic alloy prepared at 2 min. From this composition analysis confirms the growth of NPs and the presence of Si and O elements, and no other elements were found [22,1].



**Figure 8.** EDS analysis of (a) Ag NPs (b) Pd NPs (c) Ag@Pd NPs combining in Psi synthesis with different immersion time 2 and 4 min. Inset tables of figs. display the part of the each element on the sample surface.

#### 4. CONCLUSION

Ag NPs/macro Psi, Pd NPs/macro Psi and Ag@Pd NPs/macro Psi were easily obtained through an ion reduction process of salt solutions  $\text{AgNO}_3$  and  $\text{PdCl}_2$ . The structure of these NPs could be adjusted by changing the ratio of dangling bonds (Si-H) groups (growth sites) in the Psi substrates. Both the Ag and Pd in the Ag@Pd NPs are in the metallic state, Ag and Pd nanoparticles were deposited in the outer pore in the Si matrix, while Ag@PdNPs/macro Psi prepared with at 4 min deposited in the inner and outer pores this is due to the high abundance of silver and palladium in the solution and increase in the dipping time these conditions lead to a large number of ions deposited on the surface of the porous silicon.

#### ACKNOWLEDGMENT

The authors thank to Razi metallurgical research center – Iran to study SEM (MIRA3 TESCAN) and EDS analyses. Financial support of the Department of Applied Sciences/University of Technology and also Nanotechnology and Advanced Materials Research Center–University of Technology.

## REFERENCES

- [1] Layla A. Wali, Khulood K. Hasan and Alwan M. Alwan. Rapid and Highly Efficient Detection of Ultra- low Concentration of Penicillin G by Gold Nanoparticles/Porous Silicon SERS Active Substrate *Spectrochimica Acta Part A: Molecular and Biomolecular Spectroscopy* **206** (2019) 31-36.
- [2] H. H. Lin, J. Mock, D. Smith, T. Gao, M. J. Sailor. Surface-Enhanced Raman Scattering from Silver-Plated Porous Silicon *J. Phys. Chem. B* **108**, 31 (2004) 11654-11659.
- [3] A. Y. Panarin, S. N. Terekhov, K. I. Kholostov, V. P. Bondarenko. SERS-Active Substrates Based on N-Type Porous Silicon *Appl. Surf. Sci.* **256**, 23 (2010) 6969-6976.
- [4] Bin Zhang, Yuan Tuan, Karine Philippot & Ning yan, Ag-Pd and CuO-Pd nanoparticles in a Hydroxy-group functionalized ionic liquids: synthesis, characterization and catalytic performance, *This journal is © The Royal Society of Chemistry 2013 J. Name.*, **00** (2013) 1-3.
- [5] Marin Kosovic, Maja Balarin, Mile Ivanda, Vedran Đerek, Marijan Marcius, Mira Ristic, Ozren Gamulin, Porous Silicon Covered with Silver Nanoparticles as Surface-Enhanced Raman Scattering (SERS) Substrate for Ultra-Low Concentration Detection, *Applied Spectroscopy*, **69**, 12 (2015).
- [6] Lihua Shi, Aiqin Wang, Tao Zhang, Bingsen Zhang, Dangsheng Su, Huanqiao Li & Yujiang Song, One-Step Synthesis of Au-Pd Alloy Nanodendrites and Their Catalytic Activity, *J. Phys. Chem. C* **117** (2013) 12526-12536.
- [7] Kriebig U & Vollmer M. *Optical Properties of Metal Clusters Springer Series in Materials Science* **25** (1995).
- [8] Bonet F, Delmas V, Grugeon S, Urbina H R, Silvert P Y & Elhsissen K T *NanoStru. Mater.* **11** (1999) 1277.
- [9] Canxia Kan<sup>1</sup>, Weiping Cai<sup>1, 3</sup>, Cuncheng Li<sup>1</sup>, Lide Zhang<sup>1</sup> & H Hofmeister<sup>2</sup>, Ultrasonic synthesis and optical properties of Au/Pd bimetallic nanoparticles in ethylene glycol, *J. Phys. D: Appl. Phys.* **36** (2003) 1609-1614.
- [10] Alwan M. Alwan<sup>1</sup>, Intisar A. Naseef, Optimization of photoluminescence properties of Porous silicon by adding gold nanoparticles, *Iraqi Journal of Science*, **58**, 1A (2017) 53-62.
- [11] Allaa A. Jabbar, Alwan M. Alwan, Adawiya J. Haider, Modifying and Fine Controlling of Silver Nanoparticle Nucleation Sites and SERS Performance by Double Silicon Etching Process, *Plasmonics*, (2017).
- [12] N. Brahiti, T. Hadjersi, H. Menari, S. Amirouche, O. El Kechai, Enhanced photocatalytic degradation of methylene blue by metal-modified silicon nanowires, *Materials Research Bulletin* **62** (2015) 30-36.
- [13] Alwan M. Alwan, Narges Z. Abdulzahra, N. M. Ahmed, N. H. A. Halim, Influence of rapid thermal oxidation process on the optoelectronic characteristics of PSI devices, *Int. J. Nanoelectronics and Materials* **2** (2009) 157-161.
- [14] Lanying Yang, Xiong Li, Xianguo Tuo, Thanh Thi Van Nguyen, Xiangang Luo, and Minghui Hong, Alloy nanoparticle plasmon resonance for enhancing broadband antireflection of laser-textured silicon surfaces, *Optics Express* **19**, S4 (2011).
- [15] Alwan Mohammed Alwana, Ali Ahmed Yousif, Layla Alag Wali, The Growth of the Silver Nanoparticles on the Mesoporous Silicon and Macroporous Silicon: a Comparative Study *Indian Journal of Pure & Applied Physics*, **55** (2013) 813-820.
- [16] Alwan M. Alwan, Adawiya J. Hayder, Allaa A. Jabbar, Study on morphological and structural properties of silver plating on laser etched silicon, *Surface & Coatings Technology* **283** (2015) 22-28.
- [17] Wei, H.-H.; Yen, C. H.; Lin, H.-W.; Tan, C.-S. *J. Supercrit. Fluids*, **81** (2013) 1.
- [18] Alwan M. Alwan, Layla A. Wali & Ali A. Yousif, Optimization of AgNPs/mesoPS Active Substrates for Ultra-LowMolecule Detection Process" *Silicon* (2018).
- [19] F. Razia, A. Irajizada, b, F. Rahimia, Investigation of hydrogen sensing properties and aging effects of Schottky like Pd/porous Sensors and Actuators *B* **146** (2010) 53-60.

- [20] Liu, J. Zhou, H. Wang, Q. Zeng, F. Kuang and Y. J. Mater. Sci., **47** (2012) 2188.
- [21] N. Brahiti, T. Hadjersi, H. Menari, S. Amirouche & O. El Kechai, Enhanced photocatalytic degradation of methylene blue by metal-modified silicon nanowires Materials Research Bulletin **62** (2015) 30–36.
- [22] Alwan M. Alwan & Amer B. Dheyab, Room temperature CO<sub>2</sub> gas sensors of AuNPs/mesopSi hybrid structures, Appl Nanosci (2017).